AAS 14-263

NAVIGATION DESIGN AND ANALYSIS FOR THE ORION CISLUNAR EXPLORATION MISSIONS

Christopher D'Souza*, Greg Holt†, Robert Gay‡, and Renato Zanetti§

This paper details the design and analysis of the cislunar optical navigation system being proposed for the Orion Earth-Moon (EM) missions. In particular, it presents the mathematics of the navigation filter. It also presents the sensitivity analysis that has been performed to understand the performance of the proposed system, with particular attention paid to entry flight path angle constraints and the ΔV performance.

INTRODUCTION

Vehicles navigating to or from the Moon usually rely on ground tracking and ground updates to perform the insertion and correction maneuvers. A natural advancement in technology is autonomy. The Orion vehicle, designed to explore space beyond LEO, is required to return the crew safely in the case of loss of communication with the ground. As such, it needs to be able to navigate autonomously, independent of ground-based measurements, utilizing on-board sensors subject to stringent mass/power/volume constraints. Since the vehicle will be carrying optical cameras, the cislunar navigation system is designed to use images obtained from these cameras, in particular star/planetary limb and planetary disk measurements. Whereas the navigation system of Orion in and below LEO is well understood, the design of the cislunar navigation system unique presents challenges.

Whereas the Orion sensor complement includes two star trackers, the star trackers being considered have a very limited field-of-view. As such, they don't lend themselves to cislunar optical navigation, which needs fields-of-view in excess of 20 degrees. Thus, optical cameras, which are already planned for situational awareness, are harnessed into a cislunar navigation role. In this paper the design of the cislunar optical navigation system being proposed for the Orion Earth-Moon (EM) missions is presented. In particular, it will present the mathematics of the navigation filter and the analysis that has been performed to understand the performance of the proposed system, with particular attention paid to entry flight path angle constraints and the DV performance.

Previus studies focused on the lunar orbit determination problem [1, 2]. Tuckness and Young consider autonomous navigation for lunar transfers [3]. Their analysis focuses on azimuth and ele-

*GN&C Autonomous Flight Systems Engineer, Aeroscience and Flight Mechanics Division, NASA Johnson Space Center EG6, 2101 NASA Parkway, Houston, Texas, 77058. chris.dsouza@nasa.gov

†Navigation Engineer, Mission Operations Directorate, NASA Johnson Space Center EG6, 2101 NASA Parkway, Houston, Texas, 77058. chris.dsouza@nasa.gov

‡GN&C Autonomous Flight Systems Engineer, Aeroscience and Flight Mechanics Division, NASA Johnson Space Center EG6, 2101 NASA Parkway, Houston, Texas, 77058. chris.dsouza@nasa.gov

§GN&C Autonomous Flight Systems Engineer, Aeroscience and Flight Mechanics Division, NASA Johnson Space Center EG6, 2101 NASA Parkway, Houston, Texas, 77058. renato.zanetti@nasa.gov

vation measurements of the Earth, Moon, and Sun. Two star-elevation measurements relative to the planet's limb provide the same kind of information as azimuth and elevation of the apparent center of the planet. However, star-elevation measurements are the preferred approach for two reasons. First, multiple stars can be processed simultaneously, and the redundant information effectively filters out some noise. Second, the method used here does not depend on the attitude of the spacecraft, or on the misalignments of the sensors, reducing the possible error sources.

This work builds on previous results presented in [4] but focuses on new analysis done to characterize the process noise, i.e. unmodeled accelerations, and the preliminary results of the EM1 navigation system design.

This investigation specifically addresses the transfer from the Moon to the Earth. In an emergency situation, during a loss of communication scenario, the primary objective is the safety of the crew. This subsequently translates into a flight-path angle requirement at entry interface (EI) for a direct entry. A direct entry, as opposed to a skip entry, reduces the risk of the capsule bouncing back into space, and allows for a greater margin on the flight-path angle at EI.

The accuracy of the flight-path angle at EI is driven by several factors including the navigation, targeting, and burn execution errors at the time of the last mid-course maneuver, and unaccounted trajectory perturbations between the last mid-course maneuver and EI. Apollo missions tolerated a maximum flight path angle error at EI of ± 1 degree, with half of this error allocated to navigation. A similar criterion is employed in this study.

Perturbations are a major source of errors in the cislunar navigation performance of Orion. In a perfect world all the sources of perturbations would be modeled in the filter dynamics. However, computational limitations preclude such extensive modeling. Therefore, the primary sources of perturbations are characterized. In particular there are three categories of unmodeled acceleration: propulsive sources, gravitational perturbations, and solar radiation pressure. Only propulsive errors are included in this analysis; the gravitational and solar radiation pressure are not included – they will be included in a future study. For EM1, the gravitational and solar radiation pressure errors are several orders of magnitude below the thrusting sources. The propulsive sources considered are: attitude deadbands, attitude slews, CO2 venting, and sublimator venting.

Linear covariance techniques are used to perform the analysis for the Orion Cislunar missions. This comports well for the navigation system design since the cislunar navigation system on Orion will be an Extended Kalman Filter. Many of the same states and dynamics used in the linear covariance analysis will be used in the on-board cislunar navigation system. A preliminary design of the cislunar navigation system is presented. This is supported by linear covariance analyses which provides navigation performance, trajectory dispersion performance and ΔV usage.

The paper is organized as follows: Section 2 will contain a brief description of linear covariance analysis. In Section 3, the navigation system will be described. Section 4 will contain a description of the perturbations used in this analysis. Section 5 will contain results of this analysis. Finally, some concluding comments will be made in Section 6.

LINEAR COVARIANCE ANALYSIS

This investigation is performed using linear covariance (LinCov) analysis techniques [5, 6]. The state vector is given by [4]

$$\mathbf{x} = \begin{Bmatrix} \mathbf{r}^{\mathrm{T}} & \mathbf{v}^{\mathrm{T}} & \boldsymbol{\theta}^{\mathrm{T}} & \mathbf{b}_m^{\mathrm{T}} & \boldsymbol{\sigma}_m^{\mathrm{T}} & \boldsymbol{\gamma}_m^{\mathrm{T}} & \mathbf{b}_r^{\mathrm{T}} & b_{st} & b_{ss,earth} & b_{ss,moon} & b_{h,earth} & b_{h,moon} \end{Bmatrix}^{\mathrm{T}}. \tag{1}$$

The nominal trajectory is obtained by integrating the nominal dynamics model with an Encke-Nystrom method [7]. Neither the rotation vector $\boldsymbol{\theta}$ nor its uncertainty are integrated in this analysis. The nominal attitude is known at any time and it does not need to be calculated. The attitude estimation error covariance is constant and is driven by the star tracker accuracy. The attitude navigation dispersion covariance is constant and is given by the attitude control dead-band. The attitude environment dispersion covariance is constant and obtained from the above two quantities assumed uncorrelated. Before the star elevation is determined, the vehicle slews in preparation for measurement acquisition. This attitude maneuver is performed by the onboard thrusters and is assumed to be instantaneous. Due to thruster misalignment, this maneuver adds uncertainty to the translational states. After the batch of measurements is available, the vehicle returns to its nominal attitude. In linear covariance analysis, the difference between the true state and the nominal state is defined as the environment dispersion

$$\delta\mathbf{x} \triangleq \mathbf{x} - \bar{\mathbf{x}}. \tag{2}$$

The difference between the estimated state and the nominal state is defined as the navigation dispersion

$$\delta\hat{\mathbf{x}} \triangleq \hat{\mathbf{x}} - \bar{\mathbf{x}}. \tag{3}$$

Finally, the difference between the true state and the estimated state, is defined as the estimation error, sometimes referred to as the onboard navigation error

$$\mathbf{e} \triangleq \mathbf{x} - \hat{\mathbf{x}}. \tag{4}$$

Following the standard Kalman filter assumptions, the difference between the nominal and estimated models is represented with zero-mean, white noise. The estimated state evolves as

$$\dot{\hat{\mathbf{x}}} = \mathbf{f}(\hat{\mathbf{x}}), \tag{5}$$

where $\mathbf{f}$ is a nonlinear function representing the system dynamics as modeled by the filter. The evolution of the nominal state is modeled as

$$\dot{\bar{\mathbf{x}}} = \bar{\mathbf{f}}(\bar{\mathbf{x}}) = \mathbf{f}(\bar{\mathbf{x}}) + \boldsymbol{\upsilon}, \tag{6}$$

where $\bar{\mathbf{f}}$ is a nonlinear function representing the state dynamics as modeled in designing the nominal trajectory. The nominal dynamics $\bar{\mathbf{f}}$ may be higher fidelity than the filter's dynamics $\mathbf{f}$. The vector $\boldsymbol{\upsilon}$ represents the dynamics modeled in the nominal trajectory but neglected in the filter models. In Kalman filtering, the difference between the true dynamics and the filter's dynamics is called process noise. While these unmodeled dynamics are not actually white noise, they are modeled as such. The power spectral density of process noise is then tuned to achieve good performance. The same procedure is used here. In order to capture the difference between the two dynamical models, $\boldsymbol{\upsilon}$ is modeled as a zero-mean white process with spectral density $\hat{\mathbf{Q}}$. The goal is to represent the increased value of the navigation dispersion during propagation due to the difference between the nominal and filter's dynamical models.

The evolution of the navigation dispersion can be approximated to first-order as

$$\delta\dot{\hat{\mathbf{x}}} = \dot{\hat{\mathbf{x}}} - \dot{\bar{\mathbf{x}}} = \mathbf{f}(\bar{\mathbf{x}} + \delta\hat{\mathbf{x}}) - \mathbf{f}(\bar{\mathbf{x}}) - \boldsymbol{\upsilon} \simeq \mathbf{F}(\bar{\mathbf{x}})\delta\hat{\mathbf{x}} - \boldsymbol{\upsilon}. \tag{7}$$

The evolution of the navigation dispersion covariance is governed by

$$\dot{\hat{\mathbf{P}}} = \mathbf{F}(\bar{\mathbf{x}})\hat{\mathbf{P}} + \hat{\mathbf{P}}\mathbf{F}(\bar{\mathbf{x}})^{\mathrm{T}} + \hat{\mathbf{Q}}. \tag{8}$$

Similarly, the true state is modeled to evolve as

$$\dot{\mathbf{x}} = \mathbf{f}(\mathbf{x}) + \boldsymbol{\nu}. \tag{9}$$

The evolution of the estimation error is given by

$$\dot{\mathbf{e}} = \dot{\mathbf{x}} - \dot{\hat{\mathbf{x}}} \simeq \mathbf{f}(\bar{\mathbf{x}}) + \mathbf{F}(\bar{\mathbf{x}})(\mathbf{x} - \bar{\mathbf{x}}) + \boldsymbol{\nu} - \mathbf{f}(\bar{\mathbf{x}}) - \mathbf{F}(\bar{\mathbf{x}})(\hat{\mathbf{x}} - \bar{\mathbf{x}}) = \mathbf{F}(\bar{\mathbf{x}})\mathbf{e} + \boldsymbol{\nu}. \tag{10}$$

Vector $\boldsymbol{\nu}$ is modeled as zero mean white noise with spectral density $\mathbf{Q}$. The onboard covariance $\mathbf{P}$ evolves as

$$\dot{\mathbf{P}} = \mathbf{F}(\bar{\mathbf{x}})\mathbf{P} + \mathbf{P}\mathbf{F}(\bar{\mathbf{x}}) + \mathbf{Q}. \tag{11}$$

Notice that the Jacobian $\mathbf{F}$ could be evaluated at the estimated state $\hat{\mathbf{x}}$ instead of the nominal state $\bar{\mathbf{x}}$, as in the extended Kalman filter.

Finally

$$\delta\dot{\mathbf{x}} = \dot{\mathbf{x}} - \dot{\bar{\mathbf{x}}} \simeq \mathbf{F}(\bar{\mathbf{x}})\delta\mathbf{x} + \boldsymbol{\nu} - \boldsymbol{\upsilon} \tag{12}$$

and $\bar{\mathbf{P}}$ evolves as

$$\dot{\bar{\mathbf{P}}} = \mathbf{F}(\bar{\mathbf{x}})\bar{\mathbf{P}} + \bar{\mathbf{P}}\mathbf{F}(\bar{\mathbf{x}}) + \bar{\mathbf{Q}}. \tag{13}$$

Notice that $\bar{\mathbf{Q}} = \mathbf{Q} + \hat{\mathbf{Q}}$ if $\boldsymbol{\nu}$ and $\boldsymbol{\upsilon}$ are assumed to be uncorrelated.

Since the environment and navigation dispersions are naturally correlated, it is intuitive to create an augmented dispersion state, whose covariance is defined as $\boldsymbol{\Pi}$

$$\boldsymbol{\Pi} \triangleq \mathrm{E}\left\{ \begin{bmatrix} \delta\mathbf{x} \\ \delta\hat{\mathbf{x}} \end{bmatrix} \begin{bmatrix} \delta\mathbf{x} \\ \delta\hat{\mathbf{x}} \end{bmatrix}^{\mathrm{T}} \right\} = \begin{bmatrix} \bar{\mathbf{P}} & \mathbf{C} \\ \mathbf{C}^{\mathrm{T}} & \hat{\mathbf{P}} \end{bmatrix}, \tag{14}$$

$$\mathbf{C} \triangleq \mathrm{E}\left\{ \delta\mathbf{x}\, \delta\hat{\mathbf{x}}^{\mathrm{T}} \right\}. \tag{15}$$

The evolution of the augmented covariance is given by

$$\dot{\boldsymbol{\Pi}} = \begin{bmatrix} \mathbf{F}(\bar{\mathbf{x}}) & \mathbf{O}_{3\times3} \\ \mathbf{O}_{3\times3} & \mathbf{F}(\bar{\mathbf{x}}) \end{bmatrix} \boldsymbol{\Pi} + \boldsymbol{\Pi} \begin{bmatrix} \mathbf{F}(\bar{\mathbf{x}}) & \mathbf{O}_{3\times3} \\ \mathbf{O}_{3\times3} & \mathbf{F}(\bar{\mathbf{x}}) \end{bmatrix}^{\mathrm{T}} + \begin{bmatrix} \bar{\mathbf{Q}} & \hat{\mathbf{Q}} \\ \hat{\mathbf{Q}} & \hat{\mathbf{Q}} \end{bmatrix}, \tag{16}$$

where it is assumed that $\boldsymbol{\nu}$ and $\boldsymbol{\upsilon}$ are uncorrelated. All error states are modeled as first order Markov processes and are assumed to be uncorrelated to each other.

Since this filter operates once Orion is away from Earth (and outside of GPS range), the primary forces governing the motion of the vehicle are the gravitational forces of the Earth, the Moon, and the Sun. The trajectory is designed taking into account all three of these bodies. Whereas the equations of motion are formulated with respect to a central body, this (central body) changes depending on which sphere of influence the vehicle is subject to.

Optical measurements were processed every 60 seconds. The optical camera had a 18 degree Field of View. The optical measurements consist of star-horizon measurements and apparent angular radius measurements. These measurements take into account when the planet is both larger than and smaller than the field of view.

There are three categories of unmodeled acceleration with which a vehicle in cislunar space has to contend: propulsive sources, gravitational perturbations, and solar radiation pressure. Only propulsive errors are included in this analysis; the gravitational and solar radiation pressure are not included – they are several orders of magnitude below the propulsive sources. The propulsive sources, therefore, can be further separated into thruster errors and ECLSS (Environmental Control and Life Support System). Thruster errors include attitude deadbanding and attitude slewing maneuvers. ECLSS sources include Pressure Swing Adsorption (PSA) (CO_2 venting), ammonia sublimator venting, and waste water venting events. EM1 will have a 'metabolic simulator' which will exercise the entire ECLSS system except for waste water vents; hence waste water venting perturbations are not included in this analysis. Table 1 contains a summary of the previously described unmodeled acceleration as well as their relative strengths.

Table 1. Type and Strength of Unmodeled Acceleration

Type of Noise	**Assumptions**	**Strength** (m^2/s^3)
Attitude Deadbanding	Jet firing every 30 minutes	2.313×10^{-11}
Attitude Slewing	50 attitude events	3.098×10^{-9}
Attitude Slewing	25 attitude events	1.601×10^{-9}
PSA Vents	Every 6-10 minutes	4.095×10^{-10}
Ammonia Sublimator	In Lunar Vicinity (0.5 hour)	CM/SM: 1.310×10^{-5}
Ammonia Sublimator	0.5 hour prior to EI	CM Only: 7.877×10^{-5}

RESULTS

The trajectory under consideration a 8 day trajectory departing on December 15, 2017. It is shown in Figure 1.

For this analysis, we included three sets of navigation concepts of operations: 1 hour optical passes, continuous optical passes, and ground tracking only passes. The second case (continuous optical navigation) serves as a bounding case to demonstrate the best performance of the navigation system were we able to get continuous measurements. Currently, it is not clear where and how the optical camera will be mounted. If it is not mounted on a pan/tilt platform, there will need to be attitude maneuvers to obtain optical imagery for navigation. For the first case, we assumed that

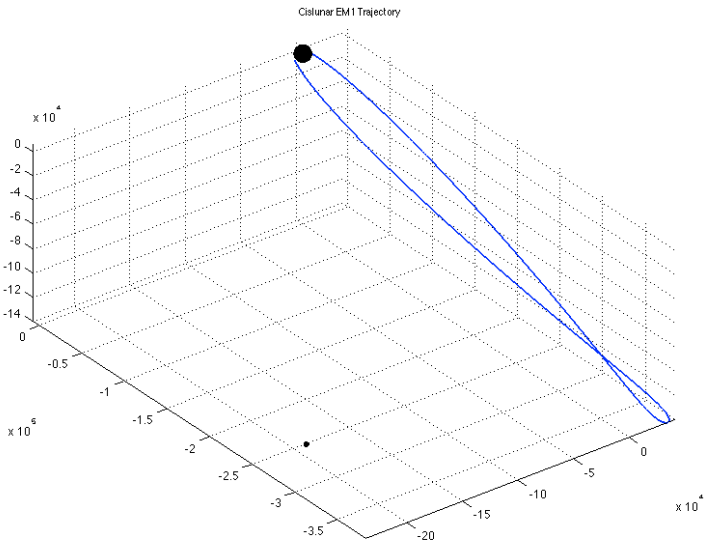

Figure 1. EM-1 Trajectory

there would be one hour of optical passes to the closest body; due to thermal and other operational constraints, we will not be able to point the cameras at the nearest body for more than an hour. This is expected to be the most reasonable optical navigation concept of operations for this scenario. In this case, we would commence tracking two hours prior to each maneuver and terminate the pass one hour prior to each maneuver. The concept of operations for ground tracking is as follows: after a period of tracking by ground stations, a navigation state (with associated covariance matrix) will be uplinked to the spacecraft one hour prior to the maneuver. This state would be used to compete and perform the maneuver. This computation of the maneuver could either be done on-board or on the ground.

The optical camera was assumed to have a noise of 5 arc-seconds (1σ) and a bias of 3.33 arc-seconds. In addition the stellar sub-point had a noise of 10 arc-seconds (1σ) and a bias of 5 arc-seconds. Finally the horizon had a noise of 10 km (1σ) and a bias of 3 km.

We assumed that there were 7 Trajectory Correction Maneuvers performed. They were chosen reflective of what was done during Apollo and will likely be adjusted, but they serve as reasonable place-holders, taking into account factors such as crew sleep and time since the previous maneuver. In order to ensure accurate delivery a maneuver was placed 6 hours prior to both Lunar Flyby and Entry Interface (EI). The TCMs are detailed in Table 2.

The TCM performance for the three cases are presented in Table 3.

The Entry Flight Path Angle (FPA) delivery (at Entry Interface) for each of these cases is included in Table 4.

Whereas one can obtain some information regarding navigation and dispersion errors in terms of position and velocity, it is most helpful and illuminating to map these (instantaneous) errors to the entry flight path angle, because that is the quantity of ultimate relevance for being able to

Table 2. TCM Locations

TCM 1	TLI + 6 hours
TCM 2	TLI + 1 day
TCM 3	Lunar Flyby - 22 hours
TCM 4	Lunar Flyby - 6 hours
TCM 5	Lunar Flyby + 18 hours
TCM 6	EI - 21 hours
TCM 7	EI - 6 hours

Table 3. 3σ TCM ΔV Performance (m/s)

	One Hour Optical	**Continuous Optical**	**Ground Tracking**
TCM 1 ΔV (m/s)	5.14	5.14	5.16
TCM 2 ΔV (m/s)	0.96	1.02	0.19
TCM 3 ΔV (m/s)	1.55	0.81	0.18
TCM 4 ΔV (m/s)	0.32	0.24	0.31
TCM 5 ΔV (m/s)	1.53	1.45	1.81
TCM 6 ΔV (m/s)	3.52	1.08	0.66
TCM 7 ΔV (m/s)	2.80	0.90	0.71
Total ΔV (m/s)	15.82	10.64	9.03

Table 4. 3σ Delivery Entry Flight Path Angle

	One Hour Optical	**Continuous Optical**	**Ground Tracking**
3 σ Entry Flight Path Angle (deg)	0.252	0.093	0.046

successfully complete the mission. This was done by means of state transition matrices, which were used to map the instantaneous navigation and dispersion errors to the time of entry interface and then using the partials of flight-path angle with respect to the state to complete the process.

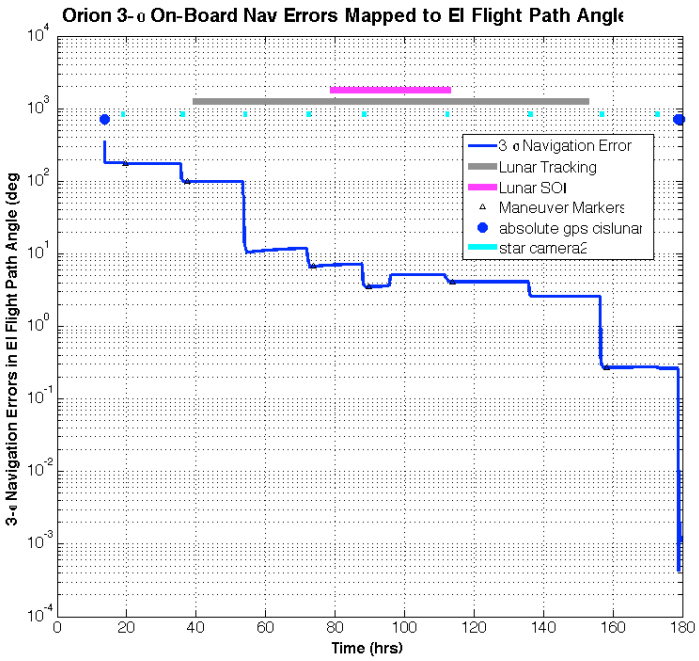

Figure 2. Entry Flight Path Angle Navigation Error (One Hour Tracking)

Sensitivity Analysis

In order to determine the 'sweet spot' of the design, a number of parameters were varied. These included: injection error accuracy, the length of optical passes, vehicle deadbanding noise, the frequency of optical measurements, and the quality of optical measurements. Each of these will be presented in turn. The metric of interest was selected to be the entry FPA dispersion. All the results will be presented in terms of this metric. In what will follow, the 'nominal' case will be as follows: a one hour optical pass prior to each maneuver with measurements taken every 60 seconds, with 50 attitude slews.

As expected, the first TCM corrects the majority of the injection error; hence the size of TCM 1 is directly proportional to the accuracy of the injection. Here the entire injection covariance matrix was scaled to determine the sensitivity It is, not surprisingly, a linear relationship. These data are presented in Table 5.

Apart from ammonia sublimator cooling, which operates for half an hour (during closest lunar approach and prior to entry), the major source of vehicle noise is the number of attitude maneuvers performed. In particular, besides increasing the size of the TCMs, this effect is of primary importance after TCM 7. Since it is not possible to know when these slews would be performed, this effect was spread out equally across the entire mission. The effect of varying the number of attitude maneuvers is seen in Table 6.

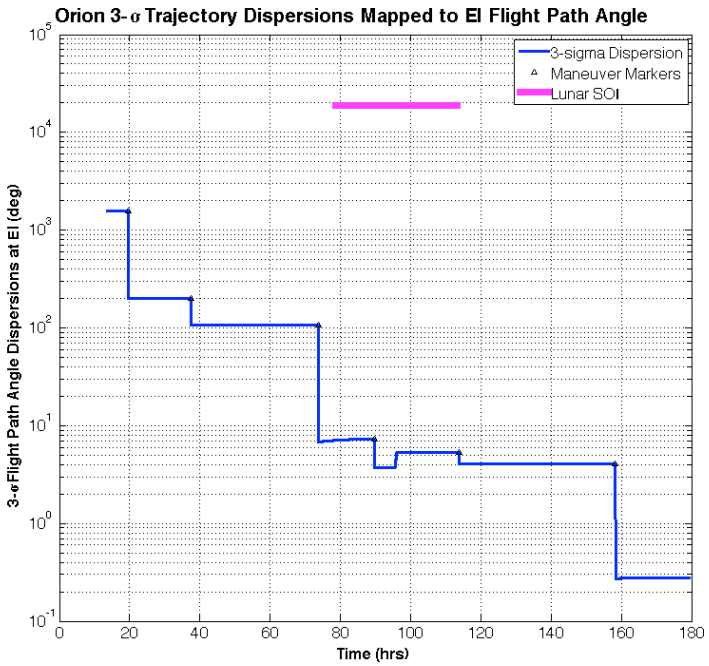

Figure 3. Entry Flight Path Angle Trajectory Dispersion Error (One Hour Tracking)

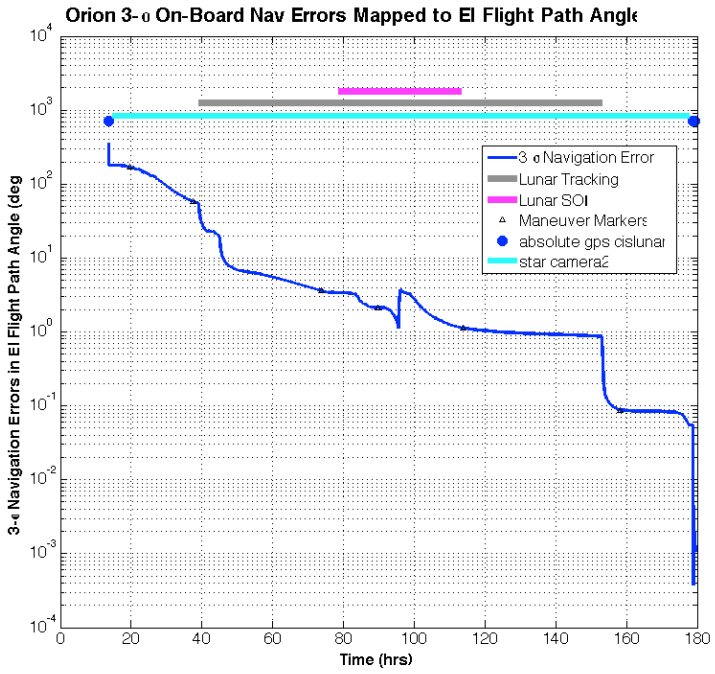

Figure 4. Entry Flight Path Angle Navigation Error (Continuous Optical Tracking)

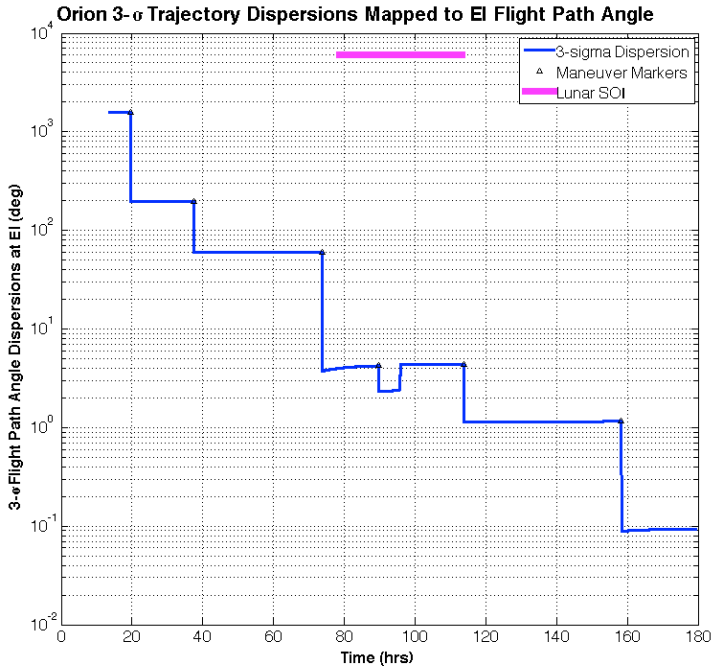

Figure 5. Entry Flight Path Angle Trajectory Dispersion Error (Continuous Optical Tracking)

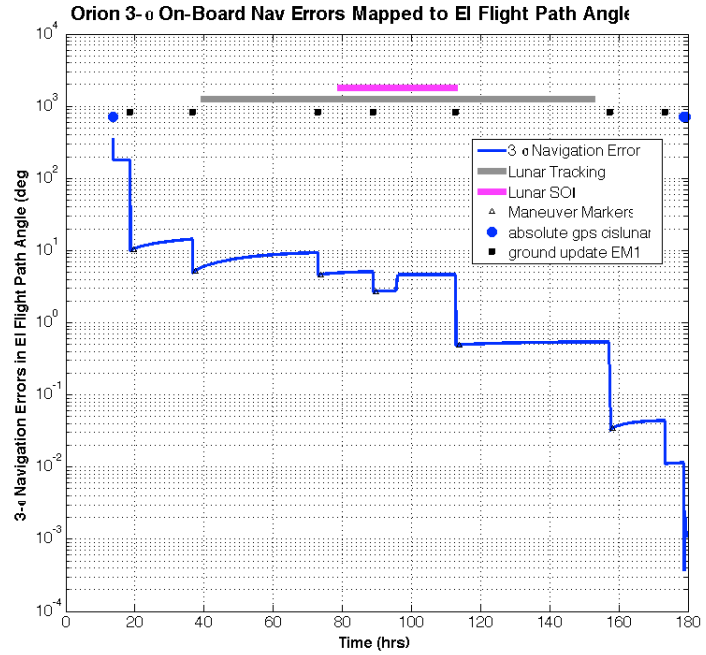

Figure 6. Entry Flight Path Angle Navigation Error (Ground Tracking Only)

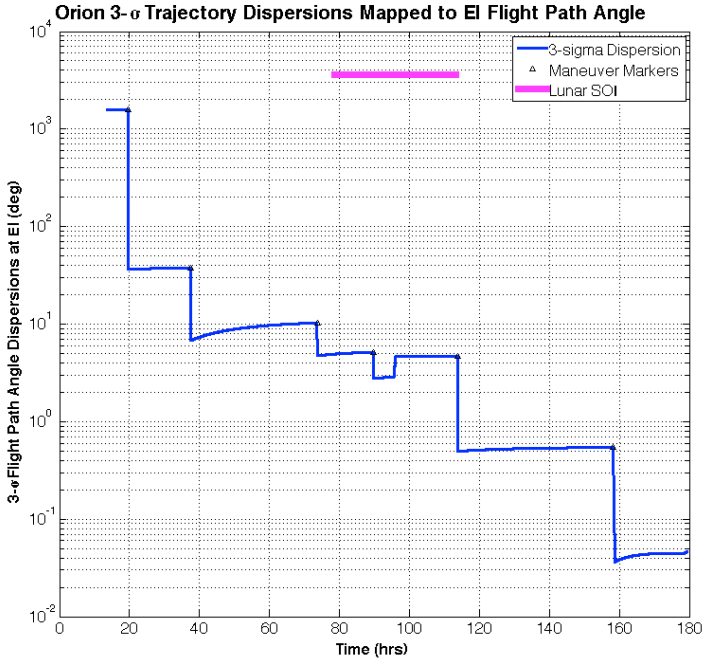

Figure 7. Entry Flight Path Angle Trajectory Dispersion Error (Ground Tracking Only)

Table 5. Sensitivity to Injection Error

	Nominal	**Half Injection Error**	**Twice Injection Error**
TCM 1 ΔV (m/s, 3σ)	5.14	2.54	10.31
TCM 2 ΔV (m/s, 3σ)	0.96	0.94	1.01
TCM 3 ΔV (m/s, 3σ)	1.55	1.53	1.56
TCM 4 ΔV (m/s, 3σ)	0.32	0.32	0.32
TCM 5 ΔV (m/s, 3σ)	1.53	1.52	1.55
TCM 6 ΔV (m/s, 3σ)	3.52	3.52	3.52
TCM 7 ΔV (m/s, 3σ)	2.80	2.80	2.80
Total ΔV (m/s, 3σ)	15.82	13.17	21.07
Entry FPA (deg, 3σ)	0.252	0.252	0.252

Table 6. Sensitivity to Attitude Maneuvers

Number of Attitude Slews	Attitude Maneuver Noise (m^2/s^3)	3σ Entry FPA Dispersion (deg)
12	7.425×10^{-10}	0.199
24	1.490×10^{-9}	0.219
36	2.231×10^{-9}	0.236
50	$\mathbf{3.098 \times 10^{-9}}$	**0.252**

We are interested in understanding the sensitivity to the measurement frequency. Hence Table 7 show the result of varying the measurement frequency from 60 seconds (the nominal) to 1 second.

Table 7. Sensitivity to Measurement Frequency

Frequency of Optical Measurements	3σ Entry FPA Dispersion (deg)
Every 60 sec	**0.252**
Every 30 sec	0.212
Every 20 sec	0.193
Every 10 sec	0.165
Every 1 sec	0.097

Next, we need to understand the effect of the measurement accuracy of the optical camera so we varied the angular accuracy as presented in Table 8.

We also wanted to determine the sensitivity of the design to the type (and duration) of the measurement source. This is presented in Table 9.

The final two factors of interest involved what happened when early TCMs and/or late TCMs were missed. Table 10 contains the entry FPA as a function of late TCMs being skipped. As can be seen, the accuracy degrades significantly as TCMs 6 and 7 are missed. Obviously, anything after 4 degrees would be outside the linear region and should be ignored.

Finally, Table **??** contains the information if early TCMs are missed. Included in here is information on the size of the remaining TCMs.

CONCLUDING COMMENTS

This paper has detailed the navigation error and trajectory dispersion sensitivity analysis for the EM-1 Free Return mission. It has determined that with one hour of tracking, the navigation performance is sufficient to meet the entry flight angle delivery error of 0.27 degrees (3 σ).

Table 8. Sensitivity to Measurement Accuracy

Quality of Optical Measurements	3σ Entry FPA Dispersion (deg)
1 arc-second	0.237
2.5 arc-seconds	0.241
5 arc-seconds	**0.252**
10 arc-seconds	0.286
20 arc-seconds	0.377
30 arc-seconds	0.472
60 arc-seconds	0.759

Table 9. Sensitivity to Type (and duration) of Measurement Source

Navigation Source	# of Attitude Maneuvers	3σ Entry FPA Dispersion (deg)
Ground Tracking Only	24	0.047
Ground Tracking w/10 min Op Pass	50	0.047
Continuous Optical	24	0.097
12 hour Optical Passes	50	0.103
8 hour Optical Passes	50	0.109
6 hour Optical Passes	50	0.121
5 hour Optical Passes	50	0.137
4 hour Optical Passes	50	0.186
2 hour Optical Passes	50	0.210
2 hour Optical Passes	**50**	**0.252**
40 minute Optical Passes	50	0.381
30 minute Optical Passes	50	0.305
20 minute Optical Passes	50	0.343
10 minute Optical Passes	50	0.436

Table 10. Sensitivity to Late TCMs being Missed

TCMs Performed	3σ Entry FPA Dispersion (deg)
[1 2 3 4 5 6 7]	**0.252**
[1 2 3 4 5 6]	0.284
[1 2 3 4 5]	4.110
[1 2 3 4]	5.332
[1 2 3]	8.324
[1 2]	127.590
[1]	209.236

Table 11. Sensitivity to Early TCMs being Missed

TCMs Performed	3σ Entry FPA Dispersion (deg)	Maneuver ΔV (3σ)
[1 2 3 4 5 6 7]	**0.252**	**15.8 (5.1, 1.0, 1.6, 0.3 1.5. 3.5, 2.8)**
[2 3 4 5 6 7]	0.252	19.1 (9.1, 1.6, 0.3, 1.8, 3.5, 2.8)
[3 4 5 6 7]	0.252	31.1 (19.8, 0.3, 4.6, 3.5, 2.9)
[4 5 6 7]	0.252	64.2 (51.0, 6.7, 3.5, 3.0)
[5 6 7]	0.252	443.3 (355.7, 17.5, 70.1)
[6 7]	0.279	3117.1 (1772.4, 1344.8)
[7]	0.317	9710.4

REFERENCES

[1] K. Hill and G. H. Born, "Autonomous Orbit Determination from Lunar Halo Orbits Using Crosslink Range," *Journal of Spacecraft and Rockets*, Vol. 45, May-June 2008, pp. 548–553.

[2] M. L. Psiaki and J. C. Hinks, "Autonomous Lunar Orbit Determination using Star Occultation Measurements," *Guidance Navigation and Control Conference and Exhibit*, Hilton Head, NC, AIAA, 20-23 August 2007.

[3] D. G. Tuckness and S.-Y. Young, "Autonomous Navigation for Lunar Transfer," *Journal of Spacecraft and Rockets*, Vol. 32, March-April 1995, pp. 279–285.

[4] R. Zanetti, "Autonomous Midcourse Navigation for Lunar Return," *Journal of Spacecrafts and Rockets*, Vol. 46, July–August 2009, pp. 865–873.

[5] P. S. Mayback, *Stochastic Models, Estimation, And Control Volume 1*. Mathematics in Science and Engineering, Orlando, FL: Academic Press, 1979.

[6] D. K. Geller, "Linear Covariance Techniques for Orbital Rendezvous Analysis and Autonomous Onboard Mission Planning," *Journal of Guidance Control and Dynamics*, Vol. 29, November-December 2006, pp. 1404–1414.

[7] R. H. Battin, *An Introduction to the Mathematics and Methods of Astrodynamics*. AIAA Education Series, New York, NY: American Institude of Aeronautics and Astronautics, 1987.